AMERICAN SOCIETY FOR MICROBIOLOGY | Journal of Virology

Entry Sites of Venezuelan and Western Equine Encephalitis Viruses in the Mouse Central Nervous System following Peripheral Infection

Aaron T. Phillips,[a,b] Amber B. Rico,[a] Charles B. Stauft,[a]* Sean L. Hammond,[b] Tawfik A. Aboellail,[a] Ronald B. Tjalkens,[b] Ken E. Olson[a]

Arthropod-Borne and Infectious Disease Laboratory, Department of Microbiology, Immunology, and Pathology, Colorado State University, Fort Collins, Colorado, USA[a]; Department of Environmental and Radiological Health Sciences, Colorado State University, Fort Collins, Colorado, USA[b]

ABSTRACT

Venezuelan and western equine encephalitis viruses (VEEV and WEEV; *Alphavirus*; *Togaviridae*) are mosquito-borne pathogens causing central nervous system (CNS) disease in humans and equids. Adult CD-1 mice also develop CNS disease after infection with VEEV and WEEV. Adult CD-1 mice infected by the intranasal (i.n.) route, showed that VEEV and WEEV enter the brain through olfactory sensory neurons (OSNs). In this study, we injected the mouse footpad with recombinant WEEV (McMillan) or VEEV (subtype IC strain 3908) expressing firefly luciferase (fLUC) to simulate mosquito infection and examined alphavirus entry in the CNS. Luciferase expression served as a marker of infection detected as bioluminescence (BLM) by *in vivo* and *ex vivo* imaging. BLM imaging detected WEEV and VEEV at 12 h postinoculation (hpi) at the injection site (footpad) and as early as 72 hpi in the brain. BLM from WEEV.McM-fLUC and VEEV.3908-fLUC injections was initially detected in the brain's circumventricular organs (CVOs). No BLM activity was detected in the olfactory neuroepithelium or OSNs. Mice were also injected in the footpad with WEEV.McM expressing DsRed (*Discosoma* sp.) and imaged by confocal fluorescence microscopy. DsRed imaging supported our BLM findings by detecting WEEV in the CVOs prior to spreading along the neuronal axis to other brain regions. Taken together, these findings support our hypothesis that peripherally injected alphaviruses enter the CNS by hematogenous seeding of the CVOs followed by centripetal spread along the neuronal axis.

IMPORTANCE

VEEV and WEEV are mosquito-borne viruses causing sporadic epidemics in the Americas. Both viruses are associated with CNS disease in horses, humans, and mouse infection models. In this study, we injected VEEV or WEEV, engineered to express bioluminescent or fluorescent reporters (fLUC and DsRed, respectively), into the footpads of outbred CD-1 mice to simulate transmission by a mosquito. Reporter expression serves as detectable bioluminescent and fluorescent markers of VEEV and WEEV replication and infection. Bioluminescence imaging, histological examination, and confocal fluorescence microscopy were used to identify early entry sites of these alphaviruses in the CNS. We observed that specific areas of the brain (circumventricular organs [CVOs]) consistently showed the earliest signs of infection with VEEV and WEEV. Histological examination supported VEEV and WEEV entering the brain of mice at specific sites where the blood-brain barrier is naturally absent.

Eastern, Venezuelan, and western equine encephalitis viruses (EEEV, VEEV, and WEEV; *Alphavirus*; *Togaviridae*) are mosquito-borne viruses in the Americas causing central nervous system (CNS) disease in humans and equids (1). EEEV, VEEV, and WEEV are maintained in nature via transmission cycles between vertebrate hosts and specific mosquito species (2). Historically, these alphaviruses have caused sporadic epizootics and epidemics in horses and humans, respectively (1, 3). Outbreaks have led to significant rates of morbidity and mortality. Survivors can suffer from debilitating and sometimes progressive neurological sequelae (4). Aspects of alphavirus-induced CNS disease remain to be fully characterized, including the specific sites of virus entry into the CNS.

WEEV strain McMillan (WEEV.McM) and other neurovirulent alphaviruses cause encephalitis in mouse infection models following aerosol, intranasal (i.n.), or subcutaneous (s.c.) challenge (1, 5, 6). We have previously shown that i.n. exposure of outbred CD-1 mice to WEEV.McM leads to virus entry into the CNS through the long axonal projections of olfactory sensory neurons (OSNs) (6, 7) and supports other studies showing that VEEV and EEEV utilize OSNs as an important route of entry into the brain following i.n. or aerosol inoculation (8–10). Alphaviruses then disseminate in the CNS along the neuronal axis, with infection of the olfactory bulb glomerular layer and lateral olfactory tract being prominent features following i.n. inoculation.

Peripheral infection with neuroinvasive alphaviruses can be modeled by s.c. inoculation of the mouse footpad. The most complete description of virus entry into the CNS comes from studies with EEEV in s.c.-injected mice and suggested that virus enters the brain directly from the bloodstream (11). Others have reported that s.c. injection of mice with VEEV leads to infection of the CNS through olfactory or peripheral nerves (12). A more recent study also supports the hypothesis that EEEV enters the CNS directly from blood following s.c. inoculation (9). However, the precise

Received 28 December 2015 **Accepted** 3 April 2016

Accepted manuscript posted online 6 April 2016

Citation Phillips AT, Rico AB, Stauft CB, Hammond SL, Aboellail TA, Tjalkens RB, Olson KE. 2016. Entry sites of Venezuelan and Western equine encephalitis viruses in the mouse central nervous system following peripheral infection. J Virol 90:5785–5796. doi:10.1128/JVI.03219-15.

Editor: S. Schultz-Cherry, St Jude Children's Research Hospital

Address correspondence to Aaron T. Phillips, aaron.phillips@colostate.edu.

* Present address: Charles B. Stauft, Codagenix, Inc., Stony Brook, New York, USA.

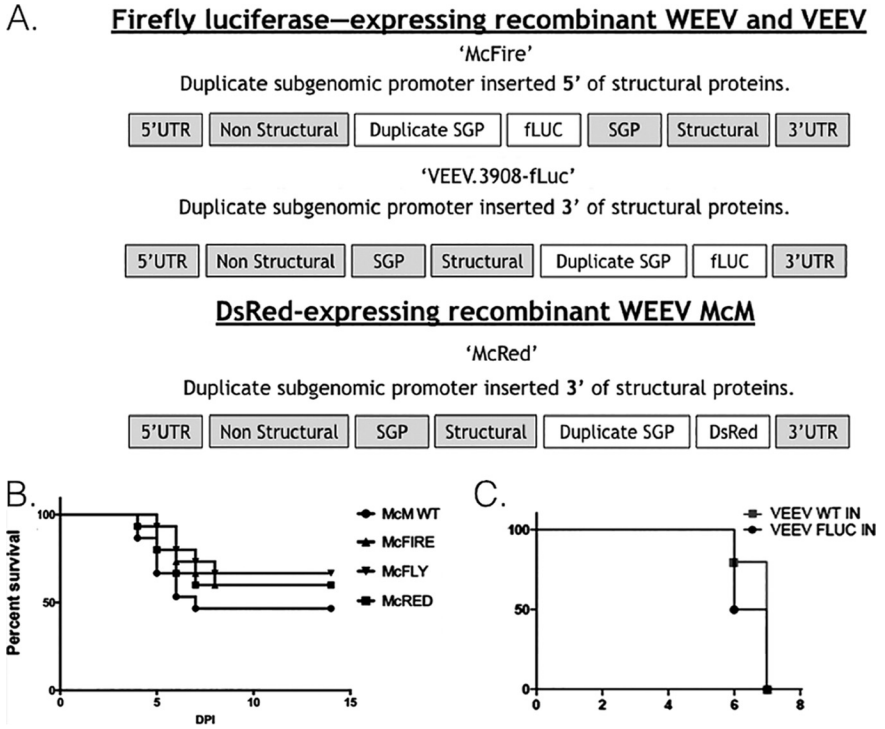

FIG 1 Recombinant alphaviruses used throughout these studies. (A) Schematic diagram illustrating the layout of the genome for each recombinant virus used in these studies. SPG, subgenomic promoter; UTR, untranslated region. (B and C) Survival of mice infected with wild-type (WT) WEEV McMillan (McM) or VEEV.3908 or recombinant WEEV or VEEV. The percentages of mice not requiring euthanasia following footpad inoculation of CD-1 mice with McM or previously published McFly, McFire, or McRed viruses (B) and VEEV.3908 and VEEV.3908-fLUC viruses (C) are shown.

entry points of WEEV or EEEV in the brain remain to be determined.

In this study, we injected the footpads of outbred CD-1 mice with alphaviruses expressing firefly luciferase (fLUC) to determine where alphaviruses enter the CNS by *in vivo* bioluminescent (BLM) imaging. We also used epifluorescence and confocal microscopy to precisely map sites of virus replication in mice using WEEV.McM expressing DsRed. Recombinant, double-subgenomic WEEV.McM or VEEV.3908 (subtype IC) expressing fLUC (13) and WEEV.McM expressing DsRed (Fig. 1A) were used in this study. At the time of our study, we did not have an EEEV expressing a marker of infection; however, mice were peripherally injected with a nonrecombinant EEEV (FL93-939) to identify sites of virus entry by immunohistochemical (IHC) approaches. We compared our *in vivo* and *ex vivo* BLM imaging studies with histological analyses of tissues to determine CNS entry points and the route of dissemination of VEEV and WEEV in the brain. Peripheral infection with each virus demonstrated a consistent spatiotemporal distribution of virus in the imaged brains. VEEV and WEEV entry occurred in areas of the CNS where the blood-brain barrier (BBB) was naturally absent. These areas included the hypothalamus and anterioventral third ventricle (AV3V) region, area postrema, and the pineal body. Virus subsequently disseminated via centripetal spread along neural pathways to other areas of the brain. These observations are consistent with a model of hematogenous seeding of virus from sites of peripheral infection and highlight previously unreported areas within the CNS, which, we hypothesize, are vulnerable to infection during viremia. These findings are important for understanding the pathogenesis of alphavirus encephalitides and should lead to a better understanding of the reported neurological sequelae among survivors of alphavirus-induced CNS disease.

MATERIALS AND METHODS

Viruses. A full-length infectious clone of the WEEV.McM was derived from a virus isolate obtained from the Arbovirus Reference Collection at the Centers for Disease Control and Prevention in Fort Collins, CO, and has been previously described (6). Passage history for virus strains used has been previously published (13, 14). Detailed descriptions of the molecular cloning methods used to construct recombinant WEEV.McM reporter viruses are provided below and have been previously published (7). In brief, we duplicated a second subgenomic promoter (SGP) sequence (nucleotides 7341 to 7500 of the viral genome) immediately 5′ of the existing SGP or immediately 3′ of the nsP4 coding region. The 5′dsWEEV.McM with fLUC inserted 5′ of the 2nd SGP is termed McFire virus in this report. The 3′dsWEEV.McM, designed to express DsRed, is referred to as McRed virus for the remainder of this report. VEEV.3908 (13), engineered to express fLUC, is designated VEEV.3908-fLUC and was designed with the 2nd SGP positioned 5′ to the structural genes. The VEEV.3908-fLUC plasmid was a kind gift from Darci Smith and Scott Weaver (University of Texas Medical Branch at Galveston).

Detailed methods for virus construction. (i) 5′sWEEV.McM.fLUC (McFire) construction. An RsrII restriction site was introduced into pWEEV.McM (6) at nucleotide 7505 (capsid gene) by PCR with overlapping primers (5′-CGT AGT AGA CAC GCA CCT ACG GAC CGC CAA AAT GTT TCC ATA CCC-3′ and 5′-GGC GGT GGG TCG GTC CGT GTC TAC TAC GTC ACC-3′). Infectious cDNA clones were treated with DpnI to remove methylated DNA and electroporated (BTX Harvard Apparatus, Holliston, MA) into *Escherichia coli* at 2,500 V, 200 Ω, and 25 μF. Transformed bacteria from each reaction were spread on LB agar with 200

μg/ml of ampicillin and incubated overnight at 37°C. Colonies were picked and grown in liquid LB medium with 200 μg/ml of ampicillin overnight at 37°C, and plasmid DNA was purified by MiniPrep (Qiagen, Valencia, CA). The full-length alphavirus subgenomic promoter (−98 to +14 nucleotides of the TAATA sequence) (15) of WEEV was amplified from pWEEV.McM using a forward primer with a 5′RsrII-SacII-SbfI multiple cloning site at the 5′ end (5′-AAA ACG GAC CGA ACC GCG GAA AAC CTG CAG GTA CTG GCA GGC CTG ATC ATC-3′) and the reverse primer used in site-directed mutagenesis. The PCR product was inserted into pMcM to generate a second subgenomic promoter 5′ of the structural genes.

(ii) 3′dsWEEV.McM.DsRed (McRed) construction. McRed virus was constructed similarly to the previously published McFly virus (7). The DsRed reporter sequence was inserted into the Age1 and FseI sites of the intermediate plasmid by engineering these sites into the PCR fragment generated from the plasmid pDsRed-monomer (Clontech, Mountain View, CA). The intermediate plasmid was digested with KpnI and MfeI, gel purified, and ligated into the KpnI- and MfeI-digested and dephosphorylated full-length infectious clone. Final plasmids were sequenced to validate proper insertion orientation.

Rescue of virus from infectious clone. VEEV and WEEV infectious clone plasmids were purified by QIAprep Spin MiniPrep kit (Qiagen, Valencia, CA), and genomic RNA was *in vitro* transcribed using a T7 RNA polymerase (MAXIscript kit; Life Technologies, Grand Island, NY). BHK-21 cells (2×10^7 in 400 μl) were transfected with 20 μl of genomic RNA using an ECM 630 electroporator (BTX Harvard apparatus; Holliston, MA). Two pulses of 450 V, 1,200 Ω, and 150 μF were administered. Rescued virus was passaged once in BHK-21 cells, collected at 48 hpi, and stored at −80°C. Stock viruses were quantified using plaque titration in Vero cells prior to experimental use. Virus titrations were performed in duplicate and plaque assays were performed as described by Liu et al. (16). Reporter gene expression (fLUC or DsRed) was confirmed in cells infected with each rescued virus.

Mouse infection and imaging. All animal protocols used in the study were reviewed and approved by the Animal Care and Use Committee at Colorado State University (permit 11-2605A). Mice were handled in compliance with the Public Health Service (PHS) policy and *Guide for the Care and Use of Laboratory Animals* (17). All experiments were conducted in a CDC select agent-approved biosafety level 3 facility. Outbred, immunocompetent CD-1 mice (female, 4 to 6 weeks old; Charles River Labs, Wilmington, MA) were used in this study. Mice were injected in the footpad with 1×10^4 PFU in a volume of 20 μl. Prior to imaging, 150 mg/kg of luciferin substrate (30-mg/ml stock) was injected (s.c.) dorsal to the cervical spine of each animal and imaged 10 to 15 min later. Uninfected mice were used as an imaging control to adjust for background signal. Mice were anesthetized with isoflurane (Minrad Inc., Bethlehem, PA) through an XGI-8 anesthesia system (Caliper Life Sciences, Waltham, MA) connected to an IVIS 200 (Caliper Life Sciences) imaging camera. Exposure time was 3 min under standard settings for the camera. Living Image 3.0 software (Caliper Life Sciences) was used to analyze and process images taken using the IVIS 200 camera. A threshold for significant BLM was established using negative imaging controls at 5×10^3 photons (p)/s/cm^2/sr. Total light emission from each mouse was determined by creating a region of interest of standard size for each mouse and collecting light emission data using the software. Mice in bisected head images were injected (s.c.) with two doses of 150 mg/kg of luciferin spaced 10 min apart prior to euthanasia. Animals were decapitated, and whole heads were bisected along the medial sagittal plane, rinsed with phosphate-buffered saline (PBS), and promptly imaged.

Immunohistochemistry. Paraffin-embedded formalin-fixed tissue was rehydrated, treated with Tris-EDTA (pH 9.0) at 90°C for 15 min, and blocked with SuperBlock T20 (Thermo, Rockford, IL). Biotinylated polyclonal rabbit anti-fLUC antibody (Abcam, Cambridge, MA) was used at a 1:1,000 dilution and incubated overnight at 4°C. Primary antibody was washed three times with Tris-buffered saline containing 0.03% Tween 20 (TBST). Sections were treated with a secondary anti-rabbit antibody conjugated with streptavidin-horseradish peroxidase (streptavidin-HRP; Rockland, Gilbertsville, PA) at a 1:6,000 dilution and incubated for 30 min at room temperature. Slides were washed three times with TBST. 3,3′-Diaminobenzidine (DAB) was added to the slides for 5 min. Hematoxylin was used as a counterstain. Hyperimmune horse serum generated against WEEV strain Fleming (CDC, Fort Collins, CO) was used for anti-WEEV IHC (1:600 dilution). The secondary antibody was HRP-conjugated rabbit polyclonal antibody (1:3,500 dilution) to horse IgG (heavy and light chain; Abcam, Cambridge, MA).

VEEV and WEEV antigens were detected by an antigen retrieval method for formalin-fixed and paraffin-embedded tissue sections in proteinase K (20 μg/ml) diluted in Tris-EDTA $CaCl_2$ buffer at pH 8.0 for 20 min at 37°C. Primary antibodies against VEEV strain TC-83, VR-1249AF (ATCC; 1:300 dilution), and against EEEV as monoclonal antibodies IB5c-3 and 1c1J-4 (CDC, Fort Collins, CO; both at a 1:100 dilution), were used to detect VEEV and EEEV antigen, respectively. Secondary antibody was goat anti-mouse antibody conjugated to HRP (Abcam; ab97023) used at a 1:1,000 dilution. All other conditions remained unchanged.

Imaging coronal sections of mouse brain. Formalin-fixed whole brains were cryosectioned into 400-μm sections using a Microm HM 450 (Thermo Scientific, Rockford, IL). The coronal sections were submerged for 15 min in TBS containing 0.01 mg/ml of Hoechst 33342 dye (Molecular Probes, Rockford, IL) and rinsed. Imaging was done with a BX51 microscope (Olympus, Center Valley, PA), ORCA-ER camera (Hamamatso; model C4742-95-12ERG), ProScan III stage controller (Prior, Rockland, MA), and CellSens Dimension v1.12 imaging software (Olympus, Center Valley, PA). Fluorescence was detected for DsRed, and Hoechst dye (nuclear counterstain) was imaged using a 2× air objective. Images were assembled into a montage of each coronal section using CellSens software.

CLARITY imaging. Enhanced fluorescence imaging of whole brains was done initially by forming a tissue-hydrogel hybrid as previously reported (18). Hydrogel-embedded brains were cryosectioned into 180-μm sections containing 2 ml of clearing solution (4% sodium dodecyl sulfate and 200 mM boric acid in deionized water, pH 8.5). Sections were clarified at room temperature for 4 days, with one change of clearing solution. Sections were then washed twice with 2 ml of TBS for 24 h per wash at room temperature. Washed sections were treated with TBS containing 0.01 mg/ml of Hoechst 33342 dye (Molecular Probes, Rockford, IL), washed with TBS, and mounted on positively charged glass slides (VECTASHIELD antifade mounting medium; Vector Laboratories, Burlingame, CA). Images were acquired using a BX51 microscope (Olympus, Center Valley, PA), ORCA-ER camera (Hamamatso; model C4742-95-12ERG), ProScan III stage controller (Prior, Rockland, MA), and CellSens Dimension v1.12 imaging software (Olympus). Fluorescence was detected for DsRed (McRed virus) and Hoechst dye (nuclear counterstain) using a 10× air objective. Additional images were acquired using a FluoView 1200 scanning-laser confocal microscope (Olympus).

RESULTS

Growth kinetics and BLM/viral titer correlation. Confluent monolayers of Vero, BHK-21, and C6/36 cells were infected with a multiplicity of infection (MOI) of each virus of 0.01. Growth kinetics assays showed maximal titers of 3.1×10^7 PFU/ml in BHK-21 cells, 1.5×10^7 PFU/ml in Vero cells, and 5.33×10^9 PFU/ml in C6/36 cells for McFire virus. There was no significant difference in viral propagation between 5′dsWEEV.McM and wild-type WEEV.McM viruses in Vero, BHK-21, or C6/36 cell cultures. In Vero and BHK-21 cells, however, McFire virus reached a maximal titer approximately 1 $\log_{10}$ less than WEEV.McM and 5′dsWEEV.McM. This difference in growth kinetics was not considered sufficient to discontinue use of McFire virus in animals. There was a strong correlation between viral replication and BLM activity. The correlation between virus titer and BLM was estab-

lished in cell culture using the ROI tool of the IVIS 200 system. Tenfold serial dilutions of virus starting at 10^5 PFU/ml in a 24-well plate format were layered onto confluent BHK-21 cells and imaged 8 h later. Luminescence correlated well with virus concentration added, with an R^2 value of 0.9673. The growth kinetics of McRed virus in cell culture (Vero cells) was compared to those of McM, McFire, and McFly viruses and found to be similar to that of wild-type virus.

Preliminary testing of recombinant alphavirus *in vivo*. After it was determined that recombinant viruses were infectious and suitable for use in animals, mortality was measured in CD-1 mice receiving footpad inoculation (Fig. 1B) and compared with those obtained with WEEV.McM, 5′dsWEEV.McM, McRed, and our previously published 3′dsWEEV.McM-fLUC (McFly) virus (7). The numbers of mice infected with each virus were as follows: wild-type virus, 24; McFire, 21; McFly, 15; and McRed, 16. Similarly, VEEV.3908-fLUC was compared to wild-type VEEV.3908 in 10 mice per virus (Fig. 1C). All recombinant viruses showed comparable rates of survival of infected CD-1 mice. Comparisons made between each group did not show statistically significant differences ($P > 0.1$). Previously published McFly virus, which had the duplicate SGP oriented 3′ of the structural genes and a large transgene (1,700 nucleotides), was not used for s.c. inoculation studies because McFire virus demonstrated better transgene retention than that of McFly (data not shown).

Distribution of DsRed in coronal slices of whole brains after McRed virus i.n. or s.c. inoculations. We next monitored infection of the CNS by the peripheral route of infection. Initially, we compared the distributions of DsRed within coronal sections of brains obtained from CD-1 mice receiving either i.n. or s.c. inoculation. Mice were euthanized soon after showing neurological signs of disease. All mice ($n = 10$) receiving i.n. inoculation required euthanasia at 3.5 days postinfection (dpi), a time frame showing great consistency for onset of CNS disease. Approximately 30% of s.c.-inoculated mice ($n = 10$) required euthanasia. The time to euthanasia increased in mice receiving footpad inoculations and ranged from 4 to 7 dpi. Mouse brains were harvested and prepared for low-resolution imaging of whole coronal sections. Examination of the DsRed distribution among the imaged sections revealed that the fluorescence patterns were distinct among s.c.- and i.n.-inoculated animals (Fig. 2A to C). Expression of DsRed within the lateral olfactory tracts was a prominent feature observed among i.n.-inoculated animals, while s.c.-inoculated animals showed DsRed associated with the caudoputamen region.

***In vivo* and *ex vivo* BLM imaging and histological examination of McFire virus invasion of the CNS after peripheral infection.** The distinctive patterns of DsRed expression between the groups (Fig. 2A to C) suggested that McRed virus entered the CNS at different locations depending on the route of inoculation. Therefore, we examined early events associated with CNS entry of VEEV and WEEV after footpad inoculation by monitoring BLM activity in the CNS after infection with McFire or VEEV.3908-fLUC virus. Live animals were imaged daily by BLM detection. WEEV and VEEV replication was detected at 12 h postinfection (hpi) in the mouse footpad and as early as 72 hpi in the CNS (head region). Alternatively, CNS infection failed to occur and the mice never showed signs of illness (Fig. 2D). Typically, CNS infection was first detected between days 3 and 7 (Fig. 2E and F). The patterns of BLM activity appeared distinct between footpad and i.n.-inoculated animals (Fig. 2G to I). Mice receiving i.n. inoculation showed BLM activity mostly rostral to the eyes. In contrast, mice receiving s.c. inoculation showed BLM activity mostly caudal to the eyes. Additionally, VEEV-inoculated animals showed variable degrees of luciferase activity within the regional draining lymph nodes. However, the appearance of lymph node involvement by VEEV was not a prerequisite for CNS invasion. All mice exhibiting BLM activity within the head region of >10,000 p/s/cm^2/sr developed neurological signs of disease. Mice exhibiting <10,000 p/s/cm^2/sr in the head did not show neurological signs of disease and did not succumb to infection at any point during the 4-week study.

We examined the olfactory tissues at early time points postinoculation by comparing DsRed expression within the olfactory bulbs of mice infected with McRed virus by either the s.c. or i.n. route. Mice receiving s.c. inoculation did not show DsRed signal in the olfactory bulb at 2 dpi at a magnification of ×100 (Fig. 3A). Mice receiving i.n. inoculation showed robust DsRed expression at a magnification of ×20 (Fig. 3B). By 3 to 4 dpi, DsRed remained undetectable in olfactory bulb glomerular layers from s.c.-inoculated animals (Fig. 3C) but was readily detected in the olfactory bulb glomerular layers from i.n.-inoculated animals (Fig. 3D). Histological examination of nasal turbinates and olfactory nerve tissues of mice from either s.c. or i.n. inoculation also shows differences in lesions at an early (3 dpi) time point (Fig. 3E and F). Mice receiving i.n. inoculation showed severe lesions of the olfactory tract, while animals receiving s.c. inoculation showed an absence of similar lesions.

To more precisely resolve virus entry sites in the CNS, we performed a sagittal bisection of the whole head at the earliest sign of BLM activity of >10,000 p/s/cm2/sr, and brains were imaged (*ex vivo*) as described earlier. BLM activity was detected in circumventricular organs (CVOs) (Fig. 4), which have extensive vasculature, fenestrated capillaries, and a lack of a normal blood-brain barrier. CVO regions with BLM activity, compared against the Allen Brain Atlas (http://mouse.brain-map.org) (Fig. 4B), included the pineal body (Fig. 4A and D) and the area postrema (Fig. 4E). BLM activity was also detected in the organum vasculosum lamina terminalis (OVLT) and subfornical organ (SFO) (Fig. 4A, C, and F) associated with the hypothalamus. Notably, the OVLT and SFO are interconnected with the median preoptic nucleus of the hypothalamus, and together, these comprise the anterioventral third ventricle (AV3V) region of the brain (19) (Fig. 4C). BLM activity at 72 hpi was consistently absent in the cerebellum and the olfactory bulbs and immediately outside the brain, i.e., the scalp region.

Histological examinations of *ex vivo* imaged tissues further supported McFire virus entering the brain at the CVOs (Fig. 5), with evidence of moderate to severe meningoencephalitis. Pathologies were associated with the hypothalamus (Fig. 5A and B), the pineal gland (Fig. 5C and D), and the area postrema (Fig. 5E and F). Meninges and corresponding parenchyma showed moderate vascular congestion and infiltration of pleocellular exudate. Mononuclear cells (immunostained for WEEV antigen) seeded the perivascular areas in the connective tissue surrounding CVOs. Apoptosis and neuropil edema became evident in the parenchyma surrounding the CVOs by 72 to 96 h after neuroinvasion. The pathological lesions and virus distribution for brains infected with VEEV.3908-fLUC were similar to those with McFire virus, indicating that VEEV.3908-fLUC likely uses the CVOs to enter the brain in mice.

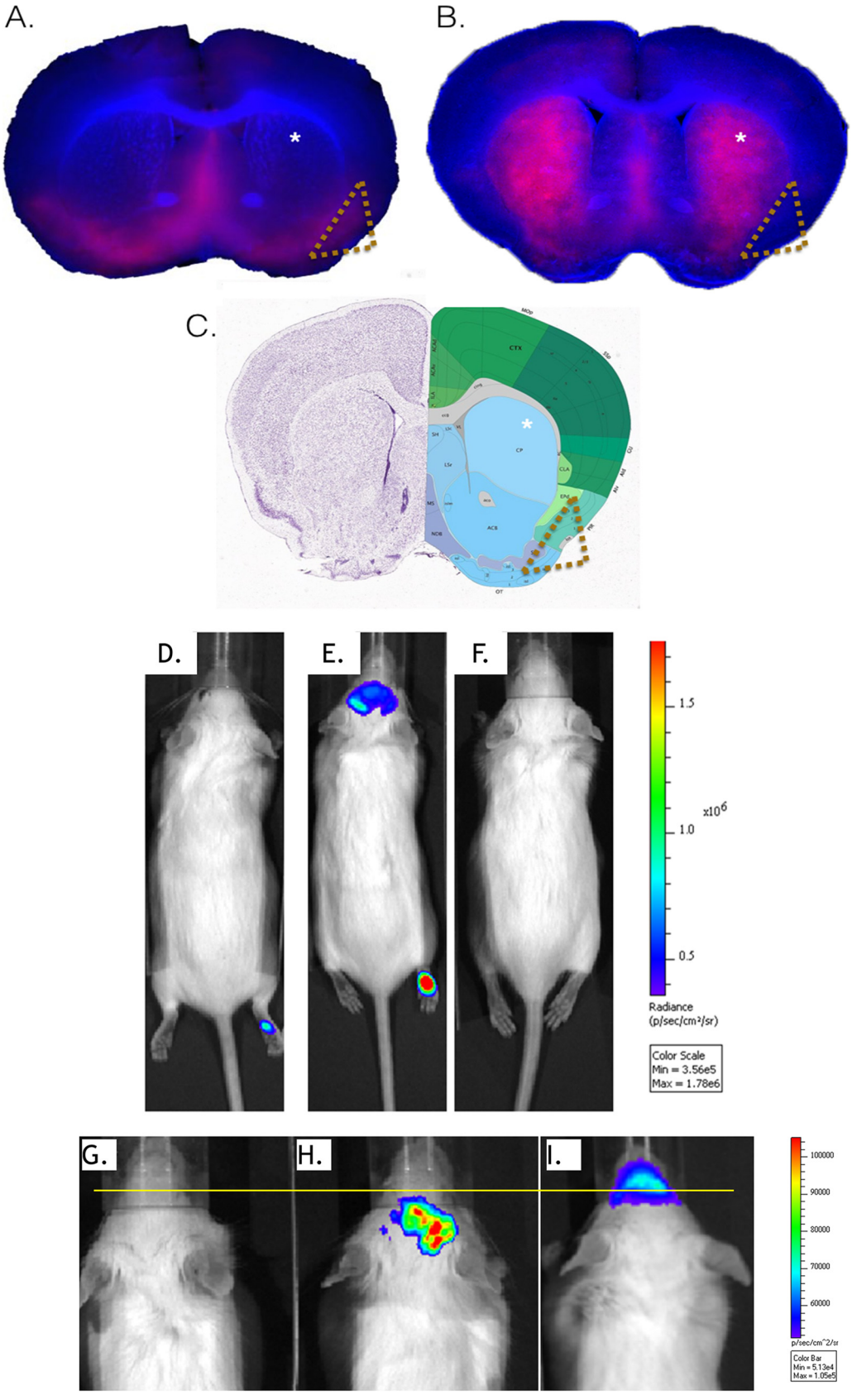
A.
B.
C.
D.
E.
F.
1.5
x10^6
1.0
0.5
Radiance
(p/sec/cm²/sr)
Color Scale
Min = 3.56e5
Max = 1.78e6
G.
H.
I.
100000
90000
80000
70000
60000
p/sec/cm^2/sr
Color Bar
Min = 5.13e4
Max = 1.05e5

Infection typically progressed along a bilateral symmetry with neurons as key targets of infection, especially in the caudate nucleus and putamen, superior and inferior colliculi, substantia nigra, hypothalamus, midbrain-tegmental region, and hindbrain. Many neurons were apoptotic, and occasional vessels in the most affected areas were cuffed by small numbers of mixed inflammatory cells, including macrophages, lymphocytes, and fewer neutrophils. Glial cells also appeared to be infected but to a lesser extent than neurons. Both astrocytes and oligodendroglial cells showed moderate WEEV antigen immunoreactivity in the most affected regions of the midbrain. Strong WEEV antigen immunoreactivity was observed in the hindbrain by 7 dpi. Apart from the brain, retinal ganglion neuronal cell bodies showed slight immunoreactivity along with scattered immunoreactivity of the retinal ganglion axons during this late-stage of disease. Cranial nerves also showed strong immunoreactivity, especially cochlear, trigeminal, and optic nerves. OSNs remained uninfected by immunochemical staining analysis.

Enhanced fluorescence imaging of McRed in CLARITY-processed coronal sections. The footpads of CD-1 mice ($n = 10$) were inoculated with McRed virus to precisely track replicating virus in the brain. Mice were euthanized at 4 dpi and whole brains subjected to CLARITY to enhance detection of DsRed in tissue sections. The initial coronal section montage (Fig. 2A and B) was opaque due to the high lipid content of the brain tissue preventing high-resolution examinations of virus entry and dissemination in the CNS. By decreasing the thickness of the tissue section (from 400 μm to 180 μm) and using the CLARITY technique of clearing lipids from tissue, we were able to visualize viral expression throughout the brain and at high resolution, including full coronal-slice montages of each section at a total magnification of ×100. Areas of interest were examined further at a total magnification of ×200 and also as confocal z-stack images.

We did not observe evidence of DsRed fluorescence in the olfactory tract at 4 dpi (Fig. 3C). Expression of DsRed was detected in internal layers of the olfactory bulb (subependymal zone) in some animals (data not shown) by 5 dpi, indicating entry into the olfactory bulb by routes not including the glomerular layer (i.e., anterograde spread). DsRed fluorescence was not detected in the glomerular layer of the olfactory bulb (Fig. 3C), an important observation, as this area has been shown to be the primary site of entry following i.n. inoculation (7). A comparison of olfactory bulbs from i.n.-inoculated animals versus s.c.-inoculated animals demonstrated this point (Fig. 3C and D). A comparison of olfactory bulb tissues from i.n.-inoculated animals versus s.c.-inoculated animals at 2 dpi (Fig. 3A and B) provides additional evidence that the routes of entry into the CNS are distinct between these inoculation routes.

Next, we identified regions where McRed virus entered the brain. Through the CLARITY method of tissue transmutation, we were able to observe the sites of virus entry at high resolution. We were able to map virus entry to the CVOs (Fig. 6). Among the CVOs, the hypothalamus and AV3V region appeared to be the most frequent route of virus entry. When neuroinvasion and CNS infection occurred, they did so at the CVOs. The CVOs include the hypothalamus and AV3V region, as well as the area postrema and pineal body. We show here that the dominant CVO to first show infection was the hypothalamus and AV3V region. A minority of animals experienced initial CNS infection in other CVO areas: the area postrema or, to a lesser frequency, the pineal body. Closer examination of this region demonstrated that neurons associated with the hypophyseal portal system of the posterior hypothalamus and pituitary, principal mammillary tract, and mammillary bodies were key targets of infection (Fig. 6A to C and F). Robust expression of DsRed was visualized throughout the principal mammillary tracts. The hypohyseal portal system and mammillary bodies are important CNS regions where neurons are in direct contact with circulating blood. The OVLT region also showed robust infection (Fig. 6D). Additionally, robust expression was present in nuclei of the substantia nigra (Fig. 6E). Cortical regions showing more faint and limited expression of DsRed were typically motor-related areas, prompting our examination of any potential retrograde spread from spinal cord neurons via the corticospinal tract. Examination of brain sections located more caudally indicated that the pyramids are devoid of DsRed fluorescence and did not support WEEV entry by corticospinal tract (Fig. 6F).

Wild-type EEEV (FL93-939) distribution in the brain is similar to that of McFire at time of neurological signs of disease. As further evidence of the central role CVOs have in alphavirus entry of the CNS, we inoculated the footpads of CD-1 mice with wild-type EEEV (FL93-939). At the time of these studies, we did not possess a reporter EEEV construct. Therefore, we relied on signs of disease to monitor infection progress. Once mice displayed neurological signs of disease, they were euthanized and their brains harvested and processed for immunohistochemistry staining. Similarly to the pattern of virus distribution in McFire-inoculated mice (Fig. 7A and B), sagittal brain sections staining positive for EEEV antigen were used to locate EEEV at specific sites within the mouse brain following EEEV challenge (Fig. 7C and D). Staining showed the presence of EEEV antigen in regions consistent with entry and infection of the CVOs. For example, viral antigen was

FIG 2 Routes of inoculation result in distinct expression patterns. The virus distributions in coronal slices of brain from CD-1 mice inoculated via intranasal or subcutaneous administration with McRed virus are shown. At the first sign of neurological disease, 7 dpi for s.c.-inoculated mice and 3.5 dpi for i.n.-inoculated mice, brains were harvested, sectioned into 400-μm coronal slices, and imaged for DsRed expression using fluorescence microscopy. Brain sections were imaged at a total magnification of ×20 for McRed (red) and nuclear counterstain (blue). Distinctive patterns of virus distribution were observed among the brains receiving virus i.n. versus s.c. Representative images show two comparable coronal sections of whole brain from animals receiving either intranasal (A) or subcutaneous (B) inoculation with McRed virus. Distinct patterns of virus distribution are marked within the caudoputamen (indicated with asterisks) and lateral olfactory tract (indicated with gold triangles). (C) An Allen Brain Atlas diagram of comparable coronal section is provided for reference. For definitions of abbreviations, see http://mouse.brain-map.org. (D to I) Whole-animal imaging showing CNS infection with McFire following footpad inoculation. CD-1 mice were inoculated in the footpad with 10^4 PFU of McFire virus and imaged daily for BLM activity (5 dpi shown). (D) Representative image shows a CD-1 mouse with no neurological signs of disease or BLM in the CNS but having detectable luciferase activity at the inoculation site. (E) Mouse with neurological signs of disease and luciferase activity within the brain region and inoculation site. (F) Uninfected control mouse. (G, H, and I) Magnified views of the head region, using the setting for the narrowest field of view, of uninfected (G), s.c.-inoculated (H), and i.n.-inoculated (I) animals. The images in panels G and H show the animal at 1 day prior to showing neurological signs of disease and required euthanasia, 5 dpi for s.c.-inoculated and 2 dpi for i.n.-inoculated animals. The yellow line is provided to allow easier visualization of signal originating rostral to the animal's eyes. Areas rostral to the eyes includes the nasal turbinates and olfactory sensory neurons.

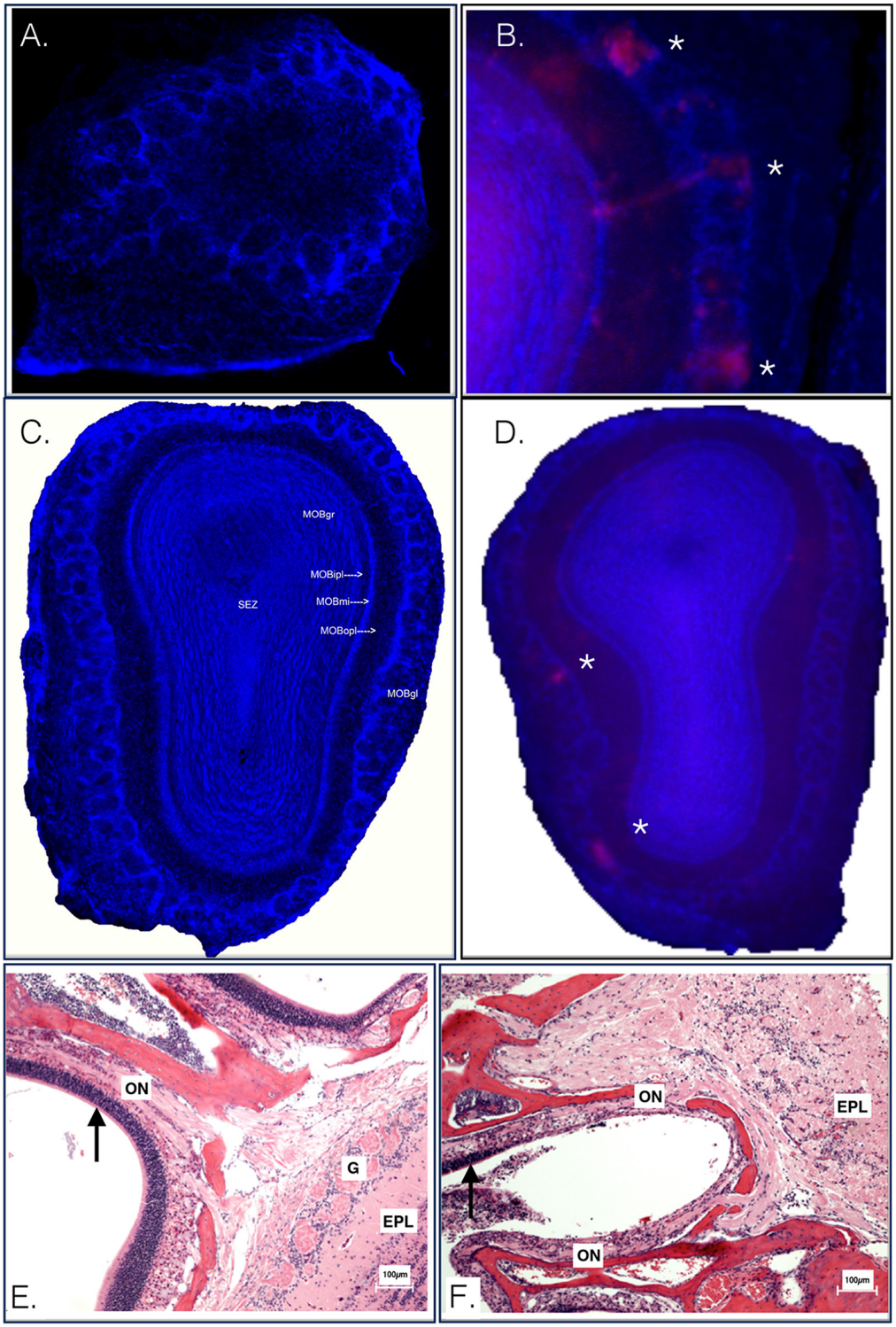

FIG 3 A closer look at the olfactory bulb at early time points postinoculation. CD-1 mice were inoculated in the footpad with McRed virus and euthanized at 2 to 5 dpi. (A) CLARITY-treated olfactory bulb section imaged at a magnification of ×100, CD-1 mouse, footpad inoculation with McRed virus, 2 dpi. McRed virus is not observed in the olfactory bulbs of s.c.-inoculated animals. (B) Olfactory bulb section imaged at a total magnification of ×2, CD-1 mouse, intranasal inoculation with McRed virus, 2 dpi. Virus was readily detectable in the olfactory bulb glomerular layers of i.n.-inoculated mice. (C) CLARITY-treated olfactory bulb section imaged at a magnification of ×100, CD-1 mouse, footpad inoculation with McRed virus, 4 dpi. The montage image shows an olfactory bulb from a mouse with severe CNS infection, the same animal as shown in Fig. 6. Note that the olfactory bulb is pristine and devoid of viral expression. (D) Representative image for comparison showing McRed virus infection in the glomerular layer (asterisks) of the olfactory bulb following i.n. inoculation, 3 dpi. (E and F) Olfactory tract of CD-1 mice inoculated s.c. (E) or i.n. (F) with VEEV.3908 72 hpi. Arrows highlight the distinct difference in the condition of the epithelium of the nasal turbinates. EPL, external plexiform layer; G, glomerular layer; ON, olfactory nerve; MOBgr, main olfactory bulb granular layer; MOBipl, main olfactory bulb internal plaexiform layer; MOBmi, main olfactory bulb mitral cell layer; MOBopl, main olfactory bulb outer plexiform layer; MOBgl, main olfactory bulb glomerular layer.

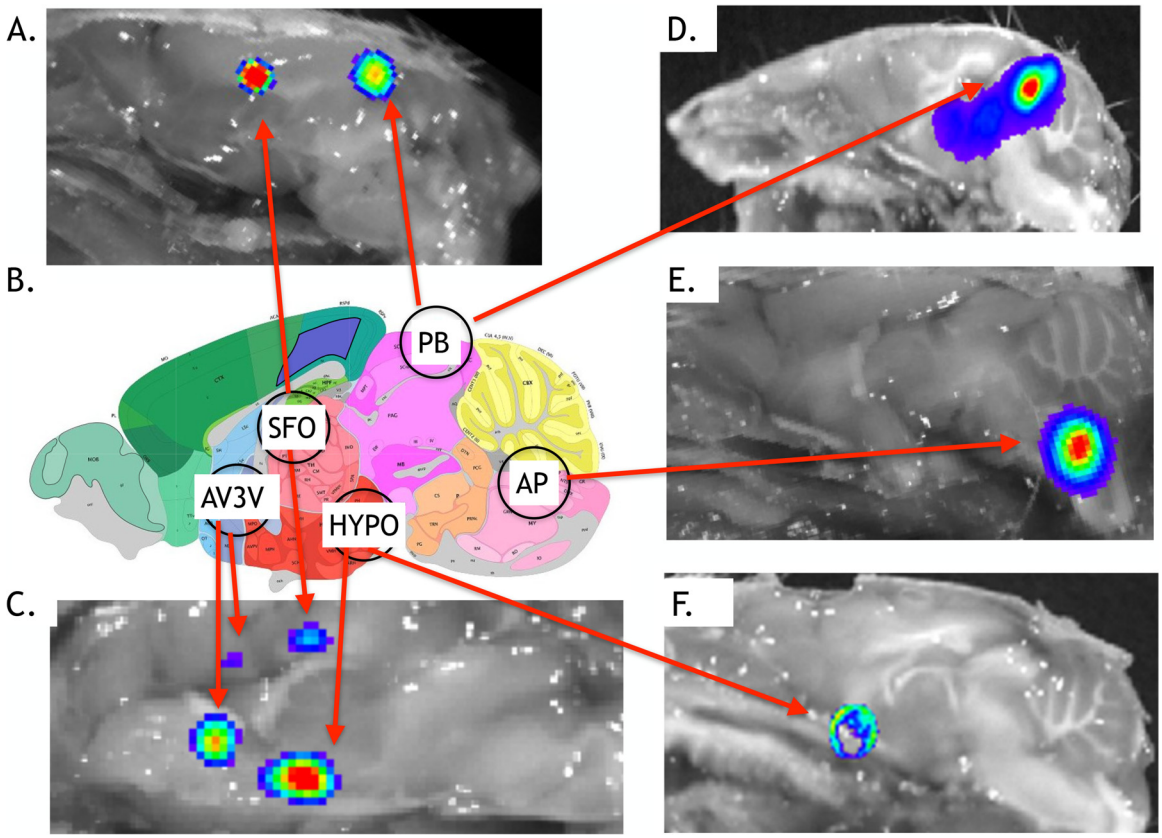

FIG 4 *Ex vivo* imaging showing early stages of CNS infection with McFire virus following footpad inoculation. CD-1 mice were challenged with 10^4 PFU of McFire virus and imaged daily for BLM activity. Following detection of increased BLM activity within the head region, mice were processed for *ex vivo* imaging. Representative images, taken at the narrowest field of view, show CD-1 mice exhibiting each of the BLM patterns observed during early stages of CNS infection (3 to 5 dpi). (A, C, and E) VEEV.3908-Fluc; (D and F) McFire virus. (B) Schematic showing the anatomical locations of the circumventricular organs (CVOs) along the sagittal axis. Circles refer to the following anatomic locations: vascular organ of the lamina terminals, subfornical organ (SFO), posterior hypothalamus (HYPO), area postrema (AP), and pineal body (PB). The vascular organ of the lamina terminals, subfornical organ, and parts of the hypothalamus make-up the anterioventral third ventricle (AV3V) region. An Allen Brain Atlas diagram of a comparable sagittal section is provided for reference. For definitions of abbreviations, see http://mouse.brain-map.org.

detected in the area postrema (Fig. 7C) and in the subfornical organ (Fig. 7D).

DISCUSSION

In this study, we inoculated 4- to 6-week-old CD-1 mice in the footpad with recombinant alphaviruses to simulate mosquito bite infection and detect early sites of virus replication in the CNS. To examine virus entry in the CNS, we used *in vivo* and *ex vivo* BLM imaging, immunohistochemical examinations, and enhanced fluorescence imaging after CLARITY. We found that VEEV, WEEV, and perhaps EEEV gain entry into the CNS at specific areas where the blood-brain barrier is naturally absent. We did not detect early BLM in CNS or ependymal tissues unassociated with CVOs, nor did we detect initial BLM signal in the olfactory bulb or associated neuroepithelium at early time points. The CVOs have not been described previously as sites of neurotropic-alphavirus entry into the CNS, increasing the significance of our findings. Interestingly, parasites have been cited as using CVOs to enter the CNS (20), indicating their potential vulnerability to pathogens as large as trypanosomes.

Our findings differ from those of earlier studies that identified VEEV entry sites after peripheral infections. Charles et al. showed that VEEV entry sites were associated with OSNs or trigeminal nerves (12). The probes used in those studies were not designed to detect viral negative-strand RNA, a sign of viral replication. We did not observe OSNs or trigeminal nerves playing a significant role in WEEV or VEEV entry by bioluminescence or fluorescence in the mouse brain. Moreover, immunochemistry staining of wild-type EEEV supported our hypothesis that hematogenous seeding of CVOs is critical to CNS invasion. We observed that the olfactory bulb can be infected later during virus dissemination in the CNS by spreading along the neuronal axis from CVO-associated entry points. The extensive neuronal connectivity known to exist among olfactory bulb or trigeminal nuclei with many other areas of the brain facilitates rapid spread of virus from the CVOs (21). Furthermore, in the studies of Charles et al. the olfactory bulb was ablated, and it was shown that the trajectory of disease was not altered after VEEV injection (12), supporting our contention that neuroinvasion occurs through CVOs. McRed virus traced the routes of virus spread, and DsRed fluorescence left a "trail" of virus replication in cells of the various brain regions identified in our study.

Alphavirus entry into the CNS in i.n.-infected mice is well established. However, no common route of neuroinvasion has been identified for virus infection from the peripheral route, and conflicting routes of neuroinvasion have been reported. Gorelkin described an

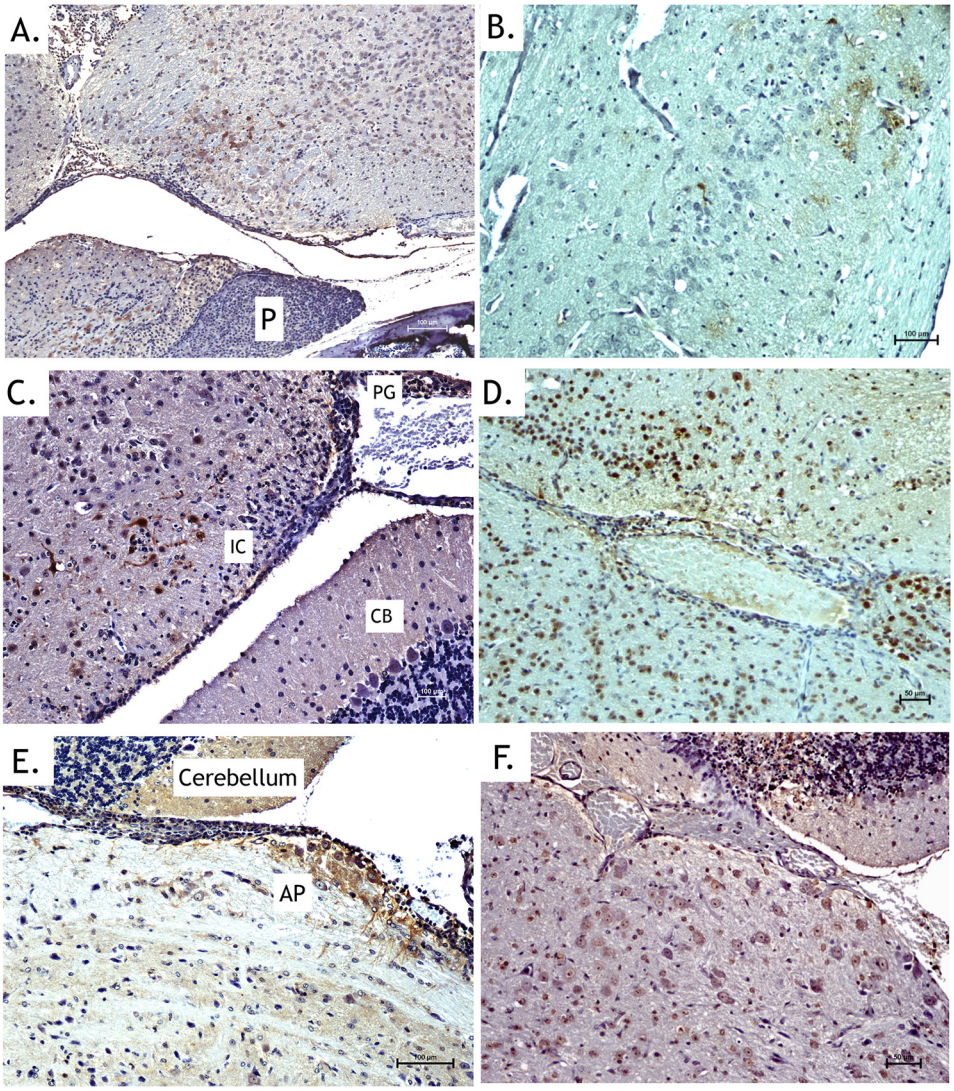

FIG 5 Immunohistochemical staining supports *in vivo* imaging results by showing entry at CVOs. Bisected heads exhibiting increased luciferase activity were processed for histological analysis. Images presented are from animals euthanized at 3 to 4 days postinoculation. (A, C, and E) Anti-WEEV antigen immunohistochemical staining (brown) of the hypothalamic region with nearby pituitary gland (A), pineal body (C), and area postrema (E) following inoculation with McFire virus. (B, D, and F) Anti-luciferase immunohistochemical staining (brown) of the hypothalamus region (B), pineal body and inferior colliculus (D), and area postrema (F) following inoculation with VEEV-3908-fLUC. No staining occurred in the anterior pituitary (P). Staining was detected in the pineal gland (PG) and nearby neurons of the inferior colliculus but not in the cerebellum (CB). Strong staining of neurons and neuronal processes was observed in the area postrema. CTX, cortex.

endothelial route for VEEV neuroinvasion, whereas, Charles et al. and Vogel et al. identified the olfactory tract as the route of invasion (12, 22, 23). Honnold et al. reported that EEEV neuroinvasion occurred through an endothelial route (9). Others have suggested alphavirus neuroinvasion from the periphery occurs by infection of leukocytes (Chikungunya virus [24]and EEEV [11]) and retrograde axonal transport (Sindbis virus [25]). The intent of the studies described here was to resolve ambiguities associated with peripheral infection and alphavirus entry of the CNS using BLM imaging and enhanced fluorescent confocal microscopy.

We have identified specific sites where alphaviruses enter the brain. These regions are collectively known as the CVOs and consist of the AV3V, posterior hypothalamus, area postrema, and the pineal body. The AV3V region is composed of the OVLT, the SFO, and the median preoptic nucleus of the hypothalamus (19). The OVLT is important in regulating blood pressure, as neurons in this region possess osmoreceptors. Neurons within the OVLT project into the hypothalamus and regulate the activity of vasopressin-secreting neurons. The SFO is also important in osmoregulation, as neurons in this region have receptors for many osmoregulatory hormones, such as angiotensin. The SFO also projects into the hypothalamus. The hypothalamus is the brain region most frequently invaded by all viruses tested, since the median eminence and neurohypophysis are both perfused by capillaries that are more permeable to macromolecules than are other CVOs (26, 27). In this study, hypothalamic neurons of the hypophyseal portal system were susceptible to alphavirus invasion (Fig. 6A and B). Hypothalamic neurons are responsible for secreting neuroendocrine hormones into the hypophyseal portal system. These neurons are in direct contact with the circulating blood and show the greatest viral

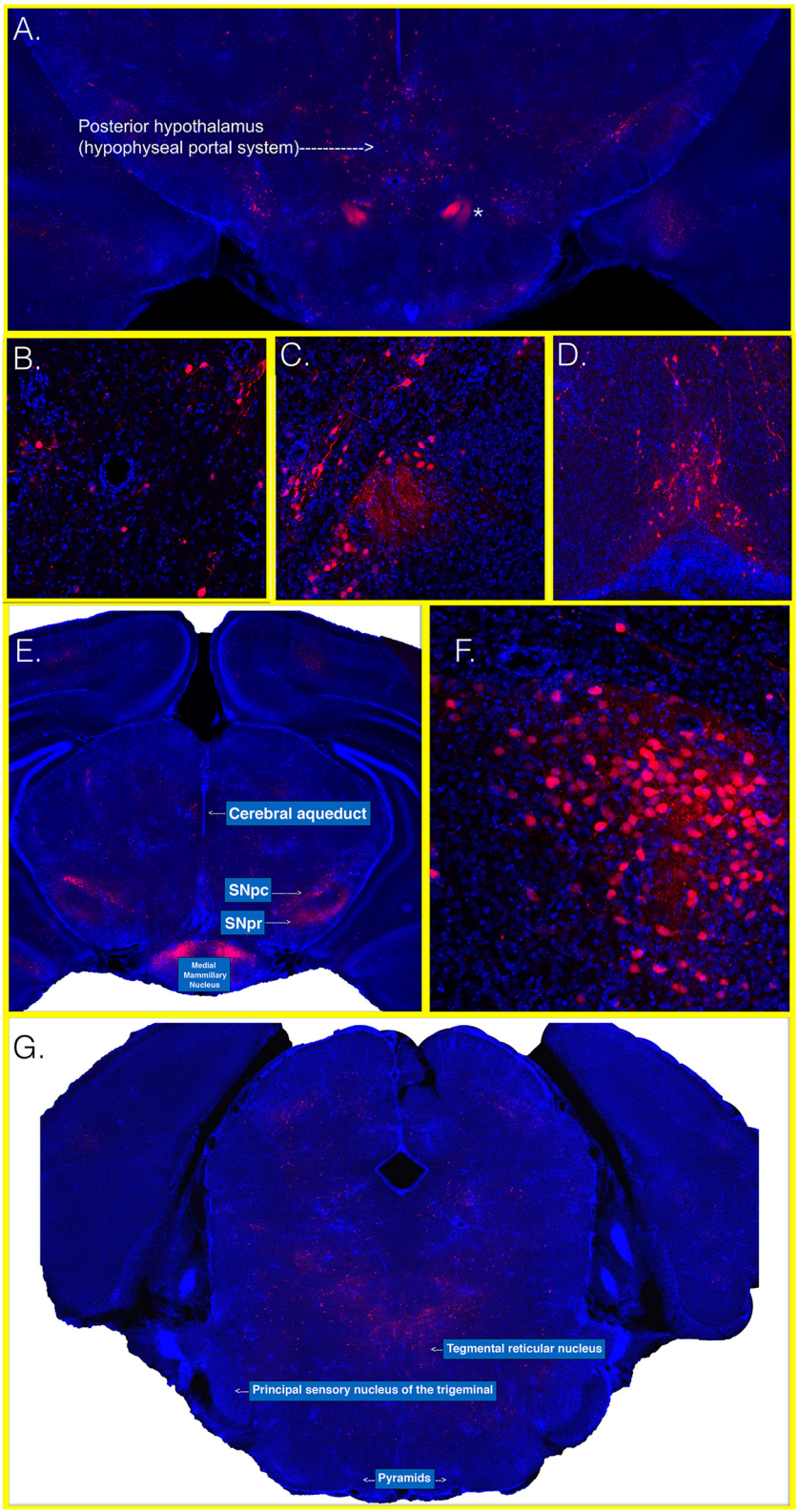

FIG 6 Images of the hypothalamus and AV3V at early time points after inoculation with McRed. CD-1 mice were inoculated in the footpad with McRed virus and euthanized at 4 dpi. Whole brains were sectioned, clarified, and imaged at a total magnification of ×100. (A) A montage image shows a coronal section and includes the hypophyseal portal system. The asterisk indicates an area consistent with the neuronal tract leading into the posterior pituitary. Areas of interest were imaged at a total magnification of ×200 and show infected neurons surrounding portal blood vessels in the hypophyseal region (B), hypothalamic nuclei with fiber tracts leading to the posterior pituitary (C), and OVLT region (D). Brain sections located more caudal show the posterior hypothalamus; midbrain nuclei show robust viral expression within nigral and mammillary nuclei (E). Mammillary nuclei were viewed at a total magnification of ×200 and show extensive infection (F). Montage imaging of coronal section, including the medullary pyramids, shows no areas of McRed virus viral expression in the corticospinal tract (pyramids) or principal sensory nucleus of the trigeminal nerve (G).

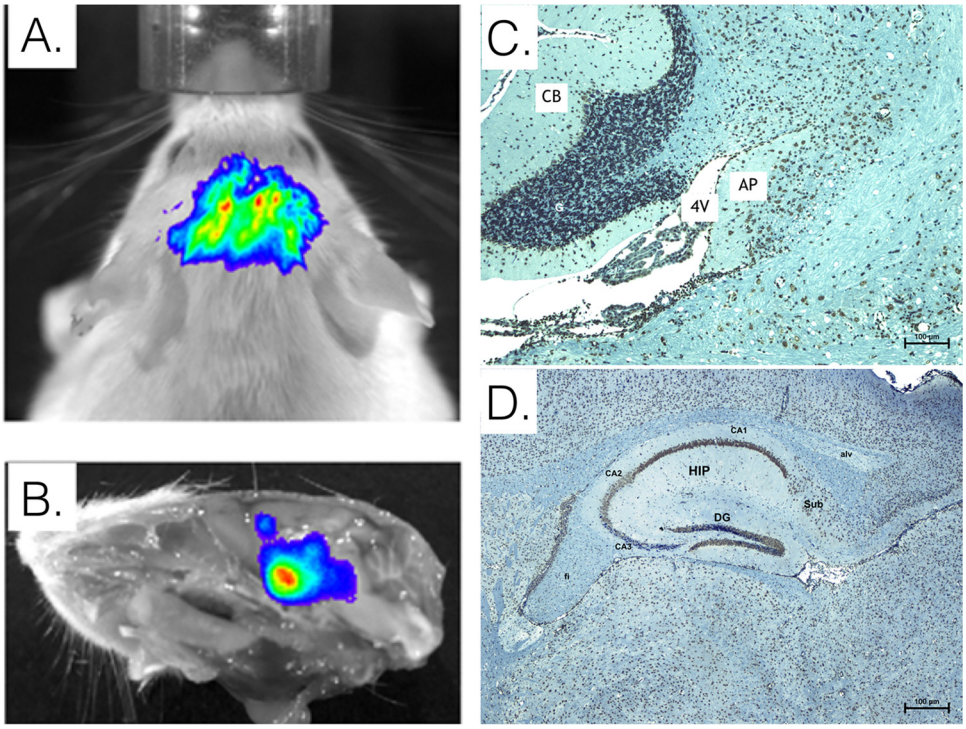

FIG 7 Histological analysis of CD-1 mouse brain tissue following peripheral inoculation with EEEV FL939 strain (4 dpi). Similar to the distribution of McFire virus at the time of neurological signs of disease (A and B), anti-EEEV immunohistochemical staining (brown) of brain tissue shows infection of area postrema region (C) and subfornical organ and hippocampal region (D). AP, area postrema; 4V, fourth ventricle; CB, cerebellum; CA1, CA2, and CA3, cornu ammonis; Sub, subiculum layer; FI, fimbria; Alv, alveus; DG, denti gyrus granular cell layer. CA1 had intense staining, CA2 had significant pathology, and CA3 had the fewest signs of pathology, especially in the caudal region; CA1 and CA2 staining was in the pyramidal layer.

expression intensity at early time points. The area postrema region monitors toxins in the blood. This highly vascularized area is responsible for stimulating the emetic response when noxious stimuli are detected within the blood and have direct contact with circulating blood. Lastly, the pineal body regulates the circadian cycle. A neuroendocrine gland itself, the pineal body was the least frequently observed route for neuroinvasion and may be a consequence of the decreased numbers of neurons compared to other CVOs (28). Less is known about the specific innervations of the pineal body.

The BBB breakdown may be important to the outcome of infection, as it is known that BBB opening occurs following inoculation with VEEV. Importantly, we failed to find multiple foci of infection during our examination of VEEV-infected mouse brains collected at early stages of CNS infection. Rather, infection followed the pathway we have described. This finding is inconsistent with BBB compromise-dependent CNS invasion by virus. We do acknowledge that other strains of VEEV, such as V3000, may vary in their capacity to compromise the BBB from peripheral sites of infection. However, we did not observe multiple foci of VEEV.3908 infection during the early time points.

Work by Schafer et al. (29) did show improvement of outcome upon treatment with inhibitors of BBB opening, although it is unclear if the treatment addresses pathogenic mechanisms subsequent to CNS invasion rather than prevention of CNS infection. It may be that the direct intracranial inoculation experiment performed in those studies induced too massive a CNS infection for the treatment to be effective in providing measurable therapeutic value. It is not clear from those studies if the treatment actually did prevent CNS infections from occurring.

Our finding that WEEV replicates within neurons of the substantia nigra recalls descriptions of neurological sequelae among survivors of WEEV-induced encephalitis. Several reports suggested that WEEV infections of humans were associated with Parkinsonism following encephalitis recovery (4, 30). Residual neurological effects can occur long after the WEEV infection has subsided and include tremor, intellectual deterioration, and cogwheel rigidity. In another study, 6 of 25 patients from a Colorado epidemic of WEEV presented with a "parkinsonian syndrome" in the form of severe, progressive neurological sequelae (31). The concept of virus-induced Parkinsonism has been reviewed in the scientific literature (32–34).

The application of bioluminescent *in vivo* imaging of whole animals and confocal fluorescence microscopy of infected and subsequently clarified brains can better define how alphaviruses interact with the mouse CNS and should benefit researchers investigating determinants of neuroinvasion independently of neurovirulence. Additionally, the identification of a route of alphavirus entry into the CNS not previously described suggests that other neuroinvasive viruses might gain entry into the CNS through similar entry sites. As newer methodologies like CLARITY (18) gain use within the neurovirology community, the visualization of viral invasion of the CNS may be possible for viruses not suitable for recombinant reporter expression.

ACKNOWLEDGMENTS

We thank Lab Animal Resources (Colorado State University) for outstanding care of the animals used in these studies, Richard Smeyne (St. Jude Children's Research Hospital) for reviewing our data for neuroanatomical accuracy, Tach Costello and Susan Rogers (Colorado State Uni-

versity) for superior administrative support, and Darci Smith for providing important reagents and stimulating discussions.

Our research has been funded by NIH grants RO1AI046435, U54AI065357, R01ES021656, and R21ES024183 and the Colorado State University DMIP Bridge Fund.

Funding sources had no role in study design; in the collection, analysis, and interpretation of data; in the writing of this review; or in the decision to submit the manuscript for publication.

FUNDING INFORMATION

This work, including the efforts of Aaron T. Phillips, Amber B. Rico, Charles B. Stauft, and Ken E. Olson, was funded by HHS | National Institutes of Health (NIH) (RO1AI046435). This work, including the efforts of Aaron T. Phillips, Amber B. Rico, Charles B. Stauft, Tawfik A. Aboellail, and Ken E. Olson, was funded by HHS | National Institutes of Health (NIH) (U54AI065357). This work, including the efforts of Aaron T. Phillips, Sean L. Hammond, Ronald B. Tjalkens, and Ken E. Olson, was funded by HHS | National Institutes of Health (NIH) (R01ES021656). This work, including the efforts of Aaron T. Phillips, Sean L. Hammond, and Ronald B. Tjalkens, was funded by HHS | National Institutes of Health (NIH) (R21ES024183). This work, including the efforts of Amber B. Rico and Ken E. Olson, was funded by Colorado State University (CSU) (Bridge Grant DMIP).

REFERENCES

1. **Steele KE, Reed DS, Glass PJ, Hart MK, Ludwig GV, Pratt WD, Parker MD, Smith JF.** 2007. Alphavirus encephalitides, p 241–254. *In* Dembek ZF (ed), Medical aspects of biological warfare. Borden Institute, Washington, DC.
2. **Weaver SC, Barrett AD.** 2004. Transmission cycles, host range, evolution and emergence of arboviral disease. Nat Rev Microbiol **2:**789–801. http://dx.doi.org/10.1038/nrmicro1006.
3. **Zacks MA, Paessler S.** 2010. Encephalitic alphaviruses. Vet Microbiol **140:**281–286. http://dx.doi.org/10.1016/j.vetmic.2009.08.023.
4. **Mulder DW, Parrott M, Thaler M.** 1951. Sequelae of western equine encephalitis. Neurology **1:**318–327. http://dx.doi.org/10.1212/WNL.1.7-8.318.
5. **Steele KE, Twenhafel NA.** 2010. Pathology of animal models of alphavirus encephalitis. Vet Pathol **47:**790–805. http://dx.doi.org/10.1177/0300985810372508.
6. **Logue CH, Bosio CF, Welte T, Keene KM, Ledermann JP, Phillips A, Sheahan BJ, Pierro DJ, Marlenee N, Brault AC, Bosio CM, Singh AJ, Powers AM, Olson KE.** 2009. Virulence variation among isolates of western equine encephalitis virus in an outbred mouse model. J Gen Virol **90:**1848–1858. http://dx.doi.org/10.1099/vir.0.008656-0.
7. **Phillips AT, Stauft CB, Aboellail TA, Toth AM, Jarvis DL, Powers AM, Olson KE.** 2013. Bioluminescent imaging and histopathologic characterization of WEEV neuroinvasion in outbred CD-1 mice. PLoS One **8:**2.
8. **Ryzhikov AB, Ryabchikova EI, Sergeev AN, Tkacheva NV.** 1995. Spread of Venezuelan equine encephalitis virus in mice olfactory tract. Arch Virol **140:**2243–2254. http://dx.doi.org/10.1007/BF01323243.
9. **Honnold SP, Mossel EC, Bakken RR, Lind CM, Cohen JW, Eccleston LT, Spurgers KB, Erwin-Cohen R, Glass PJ, Maheshwari RK.** 2015. Eastern equine encephalitis virus in mice II: pathogenesis is dependent on route of exposure. Virol J **12:**154.
10. **Koyuncu OO, Hogue IB, Enquist LW.** 2013. Virus infections in the nervous system. Cell Host Microbe **13:**379–393. http://dx.doi.org/10.1016/j.chom.2013.03.010.
11. **Vogel P, Kell WM, Fritz DL, Parker MD, Schoepp RJ.** 2005. Early events in the pathogenesis of eastern equine encephalitis virus in mice. Am J Pathol **166:**159–171.
12. **Charles PC, Walters E, Margolis F, Johnston RE.** 1995. Mechanism of neuroinvasion of Venezuelan equine encephalitis virus in the mouse. Virology **208:**662–671. http://dx.doi.org/10.1006/viro.1995.1197.
13. **Smith DR, Adams AP, Kenney JL, Wang E, Weaver SC.** 2008. Venezuelan equine encephalitis virus in the mosquito vector Aedes taeniorhynchus: infection initiated by a small number of susceptible epithelial cells and a population bottleneck. Virology **372:**176–186. http://dx.doi.org/10.1016/j.virol.2007.10.011.
14. **Phillips AT, Schountz T, Toth AM, Rico AB, Jarvis DL, Powers AM, Olson KE.** 2014. Liposome-antigen-nucleic acid complexes protect mice from lethal challenge with western and eastern equine encephalitis viruses. J Virol **88:**1771–1780. http://dx.doi.org/10.1128/JVI.02297-13.
15. **Wielgosz MM, Raju R, Huang HV.** 2001. Sequence requirements for Sindbis virus subgenomic mRNA promoter function in cultured cells. J Virol **75:**3509–3519. http://dx.doi.org/10.1128/JVI.75.8.3509-3519.2001.
16. **Liu C, Voth DW, Rodina P, Shauf LR, Gonzalez G.** 1970. A comparative study of the pathogenesis of western equine and eastern equine encephalomyelitis viral infections in mice by intracerebral and subcutaneous inoculations. J Infect Dis **122:**53–63. http://dx.doi.org/10.1093/infdis/122.1-2.53.
17. **National Research Council.** 2011. Guide for the care and use of laboratory animals, 8th ed. National Academies Press, Washington, DC.
18. **Chung K, Wallace J, Kim SY, Kalyanasundaram S, Andalman AS, Davidson TJ, Mirzabekov JJ, Zalocusky KA, Mattis J, Denisin AK, Pak S, Bernstein H, Ramakrishnan C, Grosenick L, Gradinaru V, Deisseroth K.** 2013. Structural and molecular interrogation of intact biological systems. Nature **497:**332–337. http://dx.doi.org/10.1038/nature12107.
19. **McKinley MJ.** 2003. The sensory circumventricular organs of the mammalian brain: subfornical organ, OVLT and area postrema. Springer-Verlag, Berlin, Germany.
20. **Schultzberg M, Ambatsis M, Samuelsson EB, Kristensson K, van Meirvenne N.** 1988. Spread of Trypanosoma brucei to the nervous system: early attack on circumventricular organs and sensory ganglia. J Neurosci Res **21:**56–61.
21. **Ghosh S, Larson SD, Hefzi H, Marnoy Z, Cutforth T, Dokka K, Baldwin KK.** 2011. Sensory maps in the olfactory cortex defined by long-range viral tracing of single neurons. Nature **472:**217–220. http://dx.doi.org/10.1038/nature09945.
22. **Vogel P, Abplanalp D, Kell W, Ibrahim MS, Downs MB, Pratt WD, Davis KJ.** 1996. Venezuelan equine encephalitis in BALB/c mice—kinetic analysis of central nervous system infection following aerosol or subcutaneous inoculation. Arch Pathol Lab Med **120:**164–172.
23. **Gorelkin L.** 1973. Venezuelan equine encephalomyelitis in an adult animal host. An electron microscopic study. Am J Pathol **73:**425–442.
24. **Couderc T, Chretien F, Schilte C, Disson O, Brigitte M, Guivel-Benhassine F, Touret Y, Barau G, Cayet N, Schuffenecker I, Despres P, Arenzana-Seisdedos F, Michault A, Albert ML, Lecuit M.** 2008. A mouse model for Chikungunya: young age and inefficient type-I interferon signaling are risk factors for severe disease. PLoS Pathog **4:**e29. http://dx.doi.org/10.1371/journal.ppat.0040029.
25. **Cook SH, Griffin DE.** 2003. Luciferase imaging of neurotropic viral infection in intact animals. J Virol **77:**5333–5338. http://dx.doi.org/10.1128/JVI.77.9.5333-5338.2003.
26. **Morita S, Miyata S.** 2012. Different vascular permeability between the sensory and secretory circumventricular organs of adult mouse brain. Cell Tissue Res **349:**589–603.
27. **Miyata S.** 2015. New aspects in fenestrated capillary and tissue dynamics in the sensory circumventricular organs of adult brains. Front Neurosci **9:**390.
28. **Ermisch A, Landgraf R, Rühle H-J.** 1992. Circumventricular organs and brain fluid environment: molecular and functional aspects. Elsevier, New York, NY.
29. **Schäfer A, Brooke CB, Whitmore AC, Johnston RE.** 2011. The role of the blood-brain barrier during Venezuelan equine encephalitis virus infection. J Virol **85:**10682–10690. http://dx.doi.org/10.1128/JVI.05032-11.
30. **Palmer RJ, Finley KH.** 1956. Sequelae of encephalitis; report of a study after the California epidemic. Calif Med **84:**98–100.
31. **Schultz DR, Barthal JS, Garrett C.** 1977. Western equine encephalitis with rapid onset of Parkinsonism. Neurology **27:**1095–1096. http://dx.doi.org/10.1212/WNL.27.11.1095.
32. **Henry J, Smeyne RJ, Jang H, Miller B, Okun MS.** 2010. Parkinsonism and neurological manifestations of influenza throughout the 20th and 21st centuries. Parkinsonism Relat Disord **16:**566–571. http://dx.doi.org/10.1016/j.parkreldis.2010.06.012.
33. **Jang H, Boltz DA, Webster RG, Smeyne RJ.** 2009. Viral Parkinsonism. Biochim Biophys Acta **1792:**714–721. http://dx.doi.org/10.1016/j.bbadis.2008.08.001.
34. **De Chiara G, Marcocci ME, Sgarbanti R, Civitelli L, Ripoli C, Piacentini R, Garaci E, Grassi C, Palamara AT.** 2012. Infectious agents and neurodegeneration. Mol Neurobiol **46:**614–638. http://dx.doi.org/10.1007/s12035-012-8320-7.